Chemical Physics Impact 8 (2024) 100424

Contents lists available at ScienceDirect

Chemical Physics Impact

journal homepage: www.sciencedirect.com/journal/chemical-physics-impact

Full Length Article

Synthesis, characterization and biological evaluation of novel ruthenium (II)-polypyridine mixed ligand complexes bearing 1,2,4-triazole-thiol moiety

Santhiya S [a], Arul Mary S [b], Sheeba Daniel [c,*]

[a] Department of Science and Humanities, Narayanaguru College of Engineering, Manjalumoodu, Tamil Nadu, India
[b] Department of Basic Engineering, Government Polytechnic College, Nagercoil, Tamil Nadu, India
[c] Department of Chemistry, Holy Cross College (Autonomous), Nagercoil, Tamil Nadu, India

ARTICLE INFO

Keywords:
Ru(II)-mixed ligand complexes
Antimicrobial activity
α-glucosidase inhibitory activity
SK-MEL-28 cell line
Apoptotic effect

ABSTRACT

The novel mixed ligand complexes $[Ru(bpy)_2(pytrzSH)_2](PF_6)_2$ (complex A) and $[Ru(phen)_2(pytrzSH)_2](PF_6)_2$ (complex B) (bpy = 2,2′-bipyridine, phen = 1,10-phenanthroline and pytrzSH = 5-(3-pyridyl)-4H-1,2,4-triazole-3-thiol) has been synthesized and characterized by elemental analysis, UV, FTIR, ^{1}H NMR, ^{13}C NMR and MALDI-TOF mass spectral techniques. The spectral data confirms the formation of octahedral complexes. The lipophilic nature of the complex is determined from the partition coefficient (*log* P) values and it is found to be 1.20 ± 0.004 for complex A and 1.86 ± 0.004 for complex B. The synthesised complexes show slight antimicrobial activities on *S. aureus, P. aeruginosa, E. coli, A. niger* and *C. albicans*. The α-glucosidase inhibitory activity of the synthesised complexes A and B against the positive control acarbose display IC_{50} value at 490.32 and 223.01 μg/mL. *In vitro* antiproliferative and cytotoxic effects of complexes A and B are analysed on SK-MEL-28 and non-tumoral L6 cell lines by microscopic and MTT assay methods. The IC_{50} for complexes A and B on SK-MEL-28 cancerous cell line are found to be 27.444 and 40.721 μg/mL and for non-tumoral L6 cells are 25.869 and 38.425 μg/mL respectively. The apoptotic study suggests that the synthesized complexes show late apoptotic effect on SK-MEL-28 cancerous cells and early apoptotic effect on non-tumoral L6 cells. Hence the obtained results suggest that the biological activities of the synthesised complexes depend on the nature of the ligands present in the complexes.

1. Introduction

The research on metallodrug and the success of platinum-derived anticancer drugs has been stimulated by the progress of medicinal inorganic chemistry [1–2]. The study of transition metal complexes bearing a bioactive drug is gaining more interest because of the synergetic effect of drugs on coordination with a metal [3]. This leads to the development and design of metal-based drugs with promising pharmacological applications and unique therapeutic opportunities [4–6]. The healthy human body mainly depends on the presence of metal ions for biological functions and their absence or scarcity may lead to diseases. [7,8]. Platinum complexes are considered as one of the main pillars in the chemotherapy treatment of some cancers including breast, uterine, testicular, and ovarian cancers [9]. However, administration of these compounds leads to severe problems such as neurotoxicity, nephrotoxicity, and activity against a restricted spectrum of tumors [10]. Therefore, a need for alternative metal compounds, which are presently being evaluated in clinical trials. Among the transition metal complexes, ruthenium, gallium, iron, titanium and gold complexes, ruthenium complexes are one which is regarded as promising alternatives to platinum complexes [11.12]. The Ru(II) complexes have attracted the chemists due to the combination of excellent photophysical and electrochemical properties. Ruthenium complexes are suited to rationalize anticancer drug design as that of platinum due to the high coordination number, the additional coordination sites provide the metal to fine-tune the properties of the complexes [13].

Ruthenium complexes selectively target the negatively charged components of phospholipids in the bacterial membrane and cell wall [14]. The Ru(II)-polypyridyl complexes ($[Ru(NN)_3]^{2+}$) with polypyridyl ligands have been found for developing synthetic therapeutics for

* Corresponding author.
E-mail address: sheebadaniel@holycrossngl.edu.in (S. Daniel).

https://doi.org/10.1016/j.chphi.2023.100424
Received 21 September 2023; Received in revised form 13 November 2023; Accepted 9 December 2023
Available online 10 December 2023

diabetes that exhibit hypoglycemic effects in animals and humans [15]. The development of type 2 diabetics mellitus (T2 DM) is mainly associated with the aggregation of the human islet amyloid polypeptide (hIAPP) and this phenomenon causes impaired insulin production which leads to pancreatic β-cell apoptosis. This distinctive inhibitory action of the $[Ru(NN)_3]^{2+}$ complexes is initiated by their covalent attachment to intracellular bodies of the pancreatic β-cells, which in turn modulates insulin production, therefore maintaining blood sugar levels [16].

The $[Ru(NN)_3]^{2+}$complexes having intercalating ligands are well known for their high relevance as drug candidates due to its unique properties such as chemical stability, variable oxidation states, structural diversity, low toxicity, and ability to mimic iron binding in the biological system. Some Ru complexes, NAMI-A, KP1019, and KP1339 have been evaluated in preclinical and phase I or II clinical trials and represent as a novel class of less toxic antineoplastic chemotherapeutic agents [17–19]. Lipophilicity and the charge of the ruthenium complexes are also observed to influence their biological effects [20]. The $[Ru(NN)_3]^{2+}$ complexes are potential chemotherapeutic drugs that can bind to various nucleic acid sequences in different modes, such as insertion and groove cross-binding. Thus, the complexes can be used as specific inhibitors for telomerase, DNA topoisomerase, protein kinase and so on, to regulate cell pathways and induce tumor cell apoptosis [21–23].

Similar to cisplatin, Ru(III) complexes of 1,2,4-triazole ligands act as a potential drugs for anticancer treatment and it is further treated as an alternative to the approved platinum-based anticancer drugs. The commercially available drugs of 1,2,4-triazoles such as rizatriptan which are agents for the acute treatment of migraine headaches are still considered as a topic of intensive research [24,25]. The biological properties of 1,2,4-triazole derivatives receive considerable attention due to its low toxicity, high oral bioavailability and a broad spectrum of activity. It acts as an anti-anxiety, anti-inflammatory, antimicrobial, antimycobacterial, antiviral, anticancer, antitubercular, antimycotic, analgesic, anticonvulsants, anti-nociceptive, anti-urease, antioxidant, anti-migraine, CNS stimulants and antidepressant agents [26,27]. The compound 1,2,4-triazole possesses more advantages and make them potential chemotherapeutic agents. The 1,2,4-triazole rings have not only diverse pharmacological activities but also have herbicidal, insecticidal, plant growth regulatory and antifungal activities [28,29]. Among these heterocycles, biological activities of the thiol- and thione-substituted 1,2,4-triazole systems have been reported. In addition to these important biological applications, they are also of great utility in preparative organic chemistry. Therefore 1,2,4-triazole derivatives have the chance with a good result for the research.

Metallodrugs continue as an anticancer agent in the areas of pharmaceutical research, a new way for the researchers to go for new metal-based chemotherapeutical complexes. Researchers synthesized numerous ruthenium containing complexes and tested for potential anticancer activity. An increasing number of chemo-preventive agents have been shown to stimulate apoptosis in pre-malignant and malignant cells *in vitro* or *in vivo* [30–33].

Based on the literature survey, the present work concentrates synthesis, characterization, and biological evaluation of two novel $[Ru(bpy)_2(pytrzSH)_2](PF_6)_2$ (complex A) and $[Ru(phen)_2(pytrzSH)_2](PF_6)_2$ (complex B) (bpy = 2,2′-bipyridine, phen = 1,10-phenanthroline and pytrzSH = 5-(3-pyridyl)−4H-1,2,4-triazole-3-thiol).

2. Experimental methods

$RuCl_3{\cdot}3H_2O$, bpy, phen and pytrzSH were procured from Sigma-Aldrich. All the solvents and NH_4PF_6 were procured from Merck. HPLC grade solvents and double distilled deionised water were used for the synthesis and biological studies of the complexes.

2.1. Synthesis of $[Ru(bpy)_2(pytrzSH)_2](PF_6)_2$ (Complex A)

$[Ru(bpy)_2Cl_2]$ (0.5 mM) and pytrzSH (1 mM) were dissolved in 20 mL of methanol and refluxed for 4 h under nitrogen atmosphere. The solution was then allowed to cool at room temperature and filtered to remove any insoluble impurities. A saturated solution of NH_4PF_6 was then added dropwise into the filtrate until a brown precipitate was formed. The product was filtered, washed with cold water and diethyl ether and further dried in a vacuum desiccator. Further the synthesised complex A was purified by column chromatography using silica gel as the adsorbent and a mixture of methanol and dichloromethane in the ratio of 2:8 as the eluent and on subsequent evaporation to recover the complex. The yield obtained for complex A was found to be 0.4321 g. Elemental analysis: C = 57.79%, *H* = 6.57%, *N* = 17.97% and *S* = 6.86%. The absorption maximum (λ_{max}) of complex A in acetonitrile was 476 nm. FTIR (KBr pellet): 3455, 2941, 2876, 2729, 1653, 1456, 1411, 1301, 1290, 1033, 1031, 842, 761, 729, 676, 559 and 435 cm^{-1}. ^1H NMR (DMSO-d_6, δ ppm): [bpy: 8.71 (1H, d), 8.65 (1H, d), 7.64 (1H, t),7.55 (1H, t); pytrzSH: 10.03 (1H, s), 9.21 (1H, d), 9.09 (1H, d), 8.29 (1H, d), 7.58 (2H, t), 6.5 (1H, s)]. ^{13}C NMR (DMSO-d_6, δ ppm): [bpy: 123-149 ppm; pytrzSH: 121-170 ppm]. MALDI-TOF-MS (*m/z*): complex A *m/z* is found to be 1059.703 (M^+), 914.825 ($M^{+-}PF_6$) and 769.991 ($M^{+-}2PF_6$).

2.2. Synthesis of $[Ru(phen)_2(pytrzSH)_2](PF_6)_2$ (Complex B)

$[Ru(phen)_2Cl_2]$ (0.5 mM) and pytrzSH (1 mM) were dissolved in 20 mL of methanol and refluxed for 4 h under nitrogen atmosphere. Similar procedure was carried out for the complex B synthesis as mentioned above in complex A. The yield obtained for complex B was found to be 0.4472 g. Elemental analysis: C = 60.16%, *H* = 6.46%, *N* = 16.4% and *S* = 6.42%. The absorption maximum (λ_{max}) of complex B in acetonitrile was 464 nm. FTIR (KBr pellet): 3453, 2933, 2825, 2733, 1606, 1473, 1421, 1301, 1290, 837, 745, 715, 558 and 435 cm^{-1}. ^1H NMR (DMSO-d_6, δ ppm): [phen: 7.596 - 8.865 ppm; pytrzSH: 9.994 (1H, s), 9.139 (1H, d), 9.134 (1H, d), 8.45 (1H, d), 7.57 (2H, t), 6.995 (1H, s). ^{13}C NMR (DMSO-d_6, δ ppm): [phen: 121-150 ppm; pytrzSH: 121-170 ppm]. MALDI-TOF-MS (*m/z*): complex B *m/z* is found to be 1107.885 (M^+), 963.089 ($M^{+-}PF_6$) and 817.696 ($M^{+-}2PF_6$).

2.3. Characterization techniques

The CHNS Elemental analysis of the synthesized complexes was measured using Truspec Micro Analyser. The absorption spectrum of the complexes was measured using SHIMADZU UV 1800 double beam spectrophotometer. The FTIR spectral analysis was measured using SHIMADZU FTIR double beam spectrophotometer. The ^1H and ^{13}C NMR spectra were measured using BRUCKER spectrometer. The MALDI-TOF-MS analysis was carried out to determine the *m/z* peak using Bruker Daltonics Flex-PC microflex analyser. The magnetic moment, molar conductance was measured using Guoy's balance and Systronics digital conductivity meter. The lipophillicity of the complexes was measured using shake-flask method.

2.4. Biological studies

The experimental procedure including the materials required for the antimicrobial, antidiabetic, anticancer, cytotoxicity and apoptotic studies of the synthesised complexes A and B were discussed here.

2.4.1. Antimicrobial activity

The antimicrobial activity of the ligand and the corresponding Ru(II) complexes A and B against human pathogens was carried out by agar disk diffusion method. The zone of inhibition of the ligands and the complexes on *S. aureus, E. coli, P. aeruginosa, E. faecalis, C. albicans* and *A. niger* were determined by a vernier calliper.

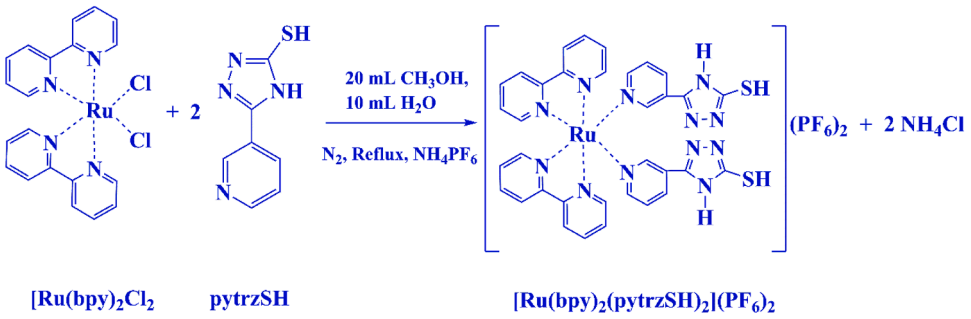

Scheme 1. Synthesis of complex A.

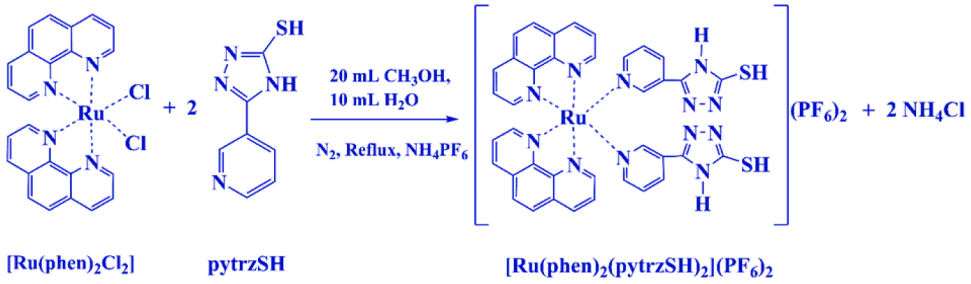

Scheme 2. Synthesis of complex B.

Table 1
MALDI-TOF mass spectral data of complexes A and B.

Complex	M^+ (m/z)	M^+ - PF_6^- (m/z)	M^+ - $2PF_6^-$ (m/z)
Complex A	1059.703	914.825	769.991
Complex B	1107.885	963.089	817.696

Table 2
Zone of inhibition of ligand and complexes A and B against bacteria.

Bacteria	Zone of Inhibition (mm)			
	Control	Ligand	Complex A	Complex B
E. faecalis	20	–	–	–
S. aureus	30	8	7	–
P. aeruginosa	25	8	7	–
E. coli	25	7	7	7

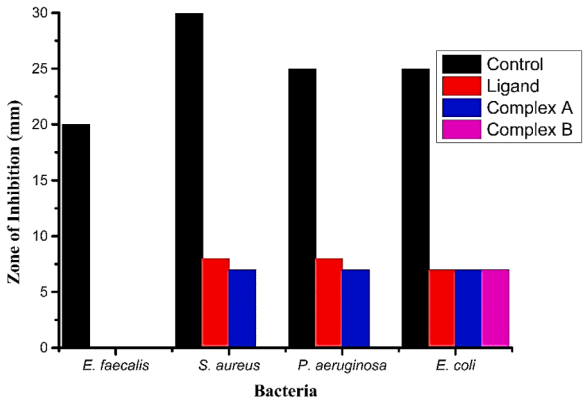

Fig. 1. Antibacterial activity of ligand and complexes.

Table 3
Zone of inhibition of ligand and complexes A and B against fungi.

Fungi	Zone of Inhibition (mm)			
	Control	Ligand	Complex A	Complex B
A. niger	20	7	–	7
C. albicans	25	–	7	10

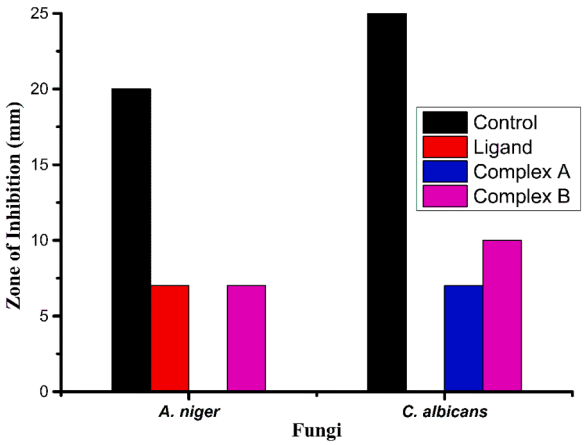

Fig. 2. Antifungal activity of ligand and complexes.

2.4.1.1. Antibacterial screening. The inoculated ligands and the complexes were evaluated for antibacterial activity against *S. aureus, E. coli, P. aeruginosa,* and *E. faecalis*. The media along with pipette, petri dishes and metallic borer were sterilized in an autoclave at 121 °C for 15 min. The culture media were finally poured into petri dishes under sterile condition. All solvent extracts were dissolved in 100% DMSO in order to achieve a concentration of 10 mg/mL. From this 10 μg/mL of complexes A and B were loaded separately into the disk and its activity was analysed. Amikacin (10 μg) was used as the positive control and DMSO was used as the negative control. All plates were incubated for 24 h at 37 °C

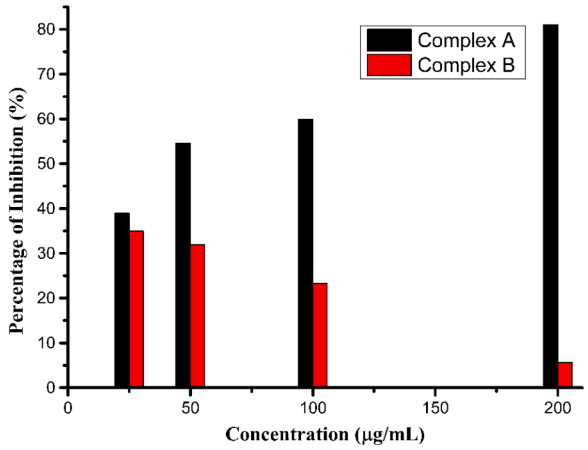

Fig. 3. Plot of percentage inhibition of α-glucosidase *vs* concentration of the complexes.

Table 4
IC_{50} value of the control and the complexes.

Complex	IC_{50} (µg/mL)
Acarbose	231.55
Complex A	490.32
Complex B	223.01

and the zone of inhibition was measured.

2.4.1.2. Antifungal screening. Antifungal activity of the ligands and the complexes were screened against *C. albicans* and *A. niger*. All samples were dissolved in DMSO to achieve a final concentration of 10 µg/mL. Nystatin was used as the positive control and DMSO as the negative control. All plates were incubated for 72 h at 30 °C and the zone of inhibition was measured in mm.

2.4.2. Determination of antidiabetic activity

The antidiabetic activity of the synthesised complexes on α-glycosidase enzymes was determined by α-glucosidase inhibitory assay. 200 µL of α-glycosidase (0.067 U/mL) was pre-incubated with different concentrations of the sample for 10 min. The substrate solution *p*-nitrophenyl glucopyranoside (pNPG) was prepared in 0.1 M sodium phosphate buffer at pH 6.9. 200 µL of 3.0 mM pNPG was then added to each of the complexes separately. The reaction mixture was incubated at 37 °C for 20 min and suspended by adding 2 mL of 0.1 M Na_2CO_3. The α-glycosidase activity of the synthesised complexes was determined by measuring the absorbance of *p*-nitrophenol released from pNPG at 400 nm. The percentage of inhibition activity was calculated from the equation:

$$\text{Percentageofinhibitoryactivity} = (B - T / B - C) \times 100$$

where B = absorbance of blank, T = absorbance of sample solution and C = absorbance of control.

2.4.3. Determination of anticancer and cytotoxic activities

Anticancer and cytotoxic activities of the complexes were analysed on SK-MEL-28 and non-tumoral L6 cell lines. SK-MEL-28 and non-tumoral L6 cell lines was initially procured from National center for Cell Sciences (NCCS), Pune, India and maintained in Dulbecco's modified Eagles medium (DMEM, Himedia). The cell line was cultured in 25 cm^2 tissue culture flask with DMEM supplemented with 10% FBS, l-glutamine, sodium bicarbonate and antibiotic solution containing penicillin (100 U/mL), streptomycin (100 µg/mL) and amphoteracin B (2.5 µg/mL). Cultured cell lines were kept at 37 ºC in a humidified 5% CO_2 incubator (Galaxy® 170 Eppendorf, Germany). The viability of cells was evaluated by direct observation of cells by inverted phase contrast microscope followed by MTT assay method.

2.4.3.1. Cell seeding in 96 well plates. Two days old confluent monolayer of SK-MEL-28 cancerous and non-tumoral L6 cell lines were trypsinized individually and the cells were suspended in 10% growth medium. 100 µL of cell suspension (5×10^4 cells/well) was seeded in 96 well tissue culture plate and incubated at 37 ºC in a humidified 5% CO_2 incubator.

2.4.3.2. Preparation of complexes. About 1 mg of complexes A and B were individually prepared by adding 1 mL of DMEM and dissolved completely by cyclomixer. The extract solution was then filtered through 0.22 µM millipore syringe filter to ensure the sterility. After 24 h the growth medium was removed, freshly prepared samples in 5% DMEM were five times serially diluted by two-fold dilution (6.25, 12.5, 25, 50 and 100 µg in 1 mL of 5% DMEM) and each complex concentration of 1 mL were added in triplicates to the respective wells and incubated at 37 ºC in a humidified 5% CO_2 incubator.

2.4.3.3. Antiproliferative effect by direct microscopic observation. The 96 well tissue culture plates along with the complexes at different concentrations were observed at different time interval from 24 to 72 h in an inverted phase contrast tissue culture microscope. The detectable changes in the morphology of the cells such as rounding or shrinking of cells, granulation and vacuolization in the cytoplasm of the cells were recorded as images under microscopic observation.

2.4.3.4. Antiproliferative effect by MTT assay method. 15 mg of MTT was reconstituted in 3 mL of phosphate-buffered saline (PBS) until completely dissolved and sterilized by filter sterilization. After 24 h of incubation period, the sample content in the wells were removed and 30 µL of reconstituted MTT solution was added to test and cell control wells, the plate was gently shaken well, then incubated at 37 ºC in a humidified 5% CO_2 incubator for 4 h After the incubation period, the supernatant solution was removed and 100 µL of MTT solubilisation solution and DMSO was added and the wells were mixed gently by pipetting up and down in order to solubilise the formazan crystals. The absorbance values were measured by using micro plate reader at a wavelength of 570 nm. The percentage of viability and growth inhibition were calculated using the equations:

$$\%\text{viability} = (\text{MeanODSamples} / \text{MeanODofcontrol}) \text{x} 100$$

$$\%\text{growthInhibition} = 100 - (\text{TreatedODsamples} / \text{Non} - \text{treatedOD}) \text{x} 100)$$

2.4.4. Apoptosis by double staining method

The morphological changes in the SK-MEL-28 and non-tumoral L6 cell lines by the addition of the synthesised complexes A and B were individually examined with DNA binding dyes acridine orange (AO) and

Table 5
Absorbance and the percentage inhibition of complexes A and B at various concentrations.

Complex	Absorbance at 25–200 (µg/mL)				% of Inhibition at 25–200 (µg/mL)			
	25	50	100	200	25	50	100	200
Complex A	0.501	0.400	0.366	0.230	38.9	54.6	59.9	81.0
Complex B	0.527	0.546	0.602	0.716	34.9	31.9	23.3	5.59

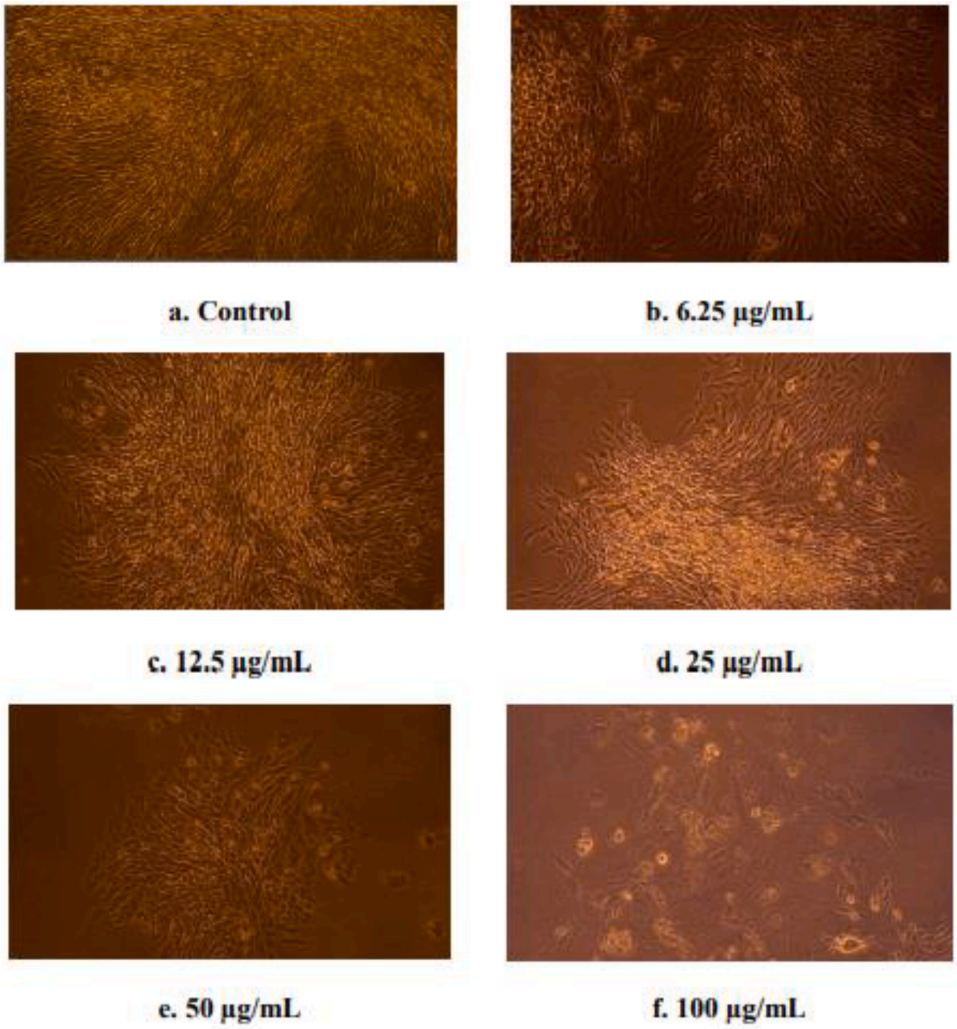

Fig. 4. Morphological changes of complex A on SK-MEL-28 cell line at various concentrations.

ethidium bromide (EB) by double staining method. The cancerous SK-MEL-28 and non-tumoral L6 cell lines were treated with IC_{50} concentration of the complexes. After 24 h incubation at CO_2 incubator, cells were washed by cold PBS and then stained with a mixture of AO (100 µg/mL) and EB (100 µg/mL) at room temperature for 10 min. The stained cells were washed twice with 1X PBS and observed by a fluorescence microscope.

3. Results and discussion

3.1. Synthesis and characterization of complexes A and B

The synthesized complexes A and B involves the coordination of Ru (II) atom individually with two bidentate bpy, phen and two mono dentate pytrzSH ligands *via* nitrogen atoms of pyridine moiety, forming an octahedral complex as shown in Schemes 1 and 2. The synthesized complexes A and B are stable solids soluble in water, acetonitrile, acetone, DMSO and DMF.

3.1.1. Elemental analysis

The percentage of C, H, N and S is determined by elemental analysis. The experimental and theoretical values for the elemental analysis of complexes A and B are in good agreement with the proposed molecular formulas $C_{34}H_{28}N_{12}S_2Ru.2PF_6$ and $C_{38}H_{28}N_{12}S_2Ru.2PF_6$ (**Table S1**).

3.1.2. Absorption spectral analysis

The absorption spectra of the synthesised complexes A and B display two spin allowed π-π* transitions at 245 and 295 nm for complex A and 227.5 and 266 nm for complex B, this is due to the presence of bpy, phen and pytrzSH ligands present in the complexes. The weak absorption bands obtained at 365.5 nm for both the complexes corresponds to the metal centered (MC) transitions. The absorptions in the region 476 nm for complex A and 464 nm for complex B are assigned due to dπ (Ru)→L metal to ligand charge transfer (MLCT) transitions. (**Fig. S1**).

3.1.3. FTIR spectral analysis

The absorption bands occur at 3455 cm^{-1} for complex A and 3453 cm^{-1} for complex B indicate the N—H stretching vibration of pytrzSH ligand. The existence of free –SH group in both the complexes are confirmed by the formation of weak bands at 2729 and 2733 cm^{-1}. The absorption bands obtained for complex A at 1653, 1456, 1411, 1301 and 761 cm^{-1} correspond to the bpy ligands. The complex B shows absorption peaks at 1606, 1473 and 1421 cm^{-1} represent the presence of phen ligands in the synthesised complex. The peaks occur at 2941 and 2876 cm^{-1} for complex A and 2933 and 2825 cm^{-1} for complex B denotes the aromatic C – H stretching vibrations of bpy, phen and pytrzSH ligands. The in-plane bending vibrations of pyridyl rings are obtained as a weak band at 1290 and 1031 cm^{-1} for complex A and 1290 cm^{-1} for complex B. Bands obtained at 1033 cm^{-1} for complex A and 1346 cm^{-1} for complex B correspond to the N—N stretching vibration of 1,2,4-triazole ring present in the pytrzSH ligand. The C-S stretching band for

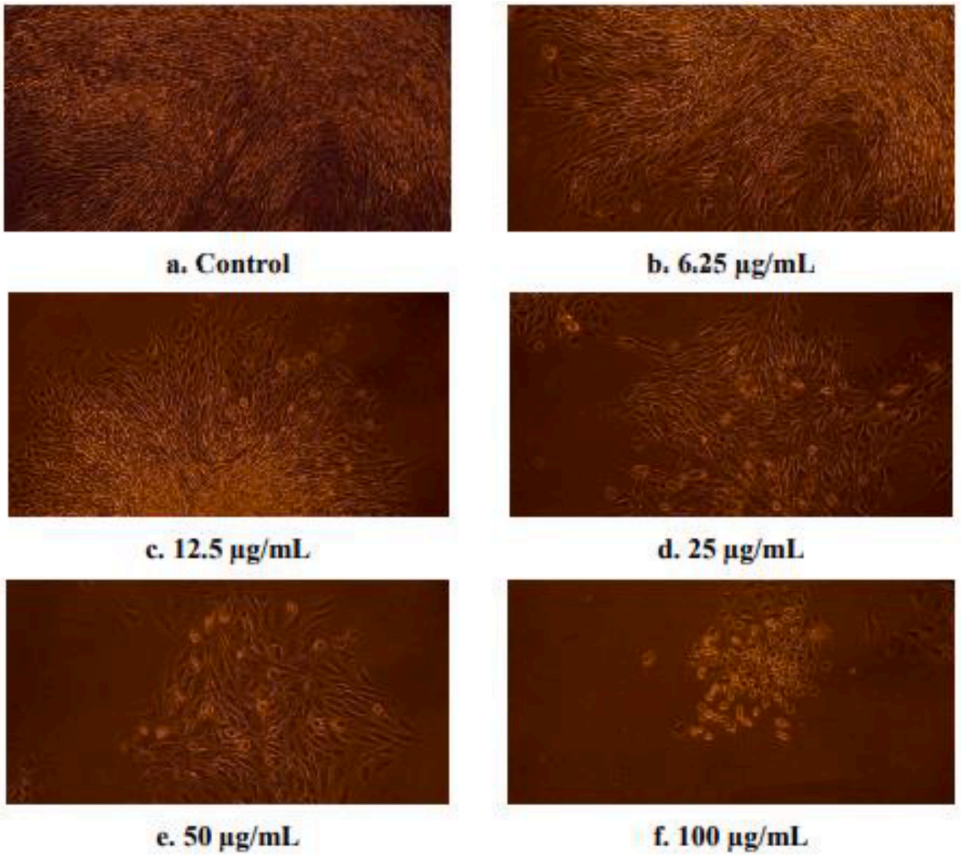

Fig. 5. Morphological changes of complex B on SK-MEL-28 cell line at various concentrations.

pytrzSH ligand is obtained at 678 cm^{-1} for complex A and 715 cm^{-1} for complex B. The bands obtained at 729, 559 and 435 cm^{-1} for complex A and 745, 558 and 435 cm^{-1} for complex B confirm the coordination of nitrogen atoms of bpy, phen and pytrzSH ligands to the central Ru metal. The weak absorption band obtained at 839–845 cm^{-1} for both the complexes A and B confirm the presence of hexafluorophosphate counter ion. Thus, the FTIR data validates the formation of complexes A and B complexes with PF_6^- counter ions (**Fig. S2**).

3.1.4. ^1H and ^{13}C NMR spectral analysis

The ^1H NMR spectrum of complex A shows the proton signals of bpy and pytrzSH ligands coordinated through the nitrogen atoms of pyridine rings to the Ru atom. The chemical shift of bpy ligand ranges from 7.553 - 8.712 ppm to the Ru metal core. The pyridine ring attached to the 5th position of 1,2,4-triazole ring present in the ancillary ligand pytrzSH shows proton signals at 9.21 ppm for H^2 proton, 8.29 ppm for H^4, 7.58 ppm for H^5 and 9.09 ppm for H^6 proton. The free –SH group present in the 3rd position and the proton attached to the nitrogen atom at 4th position of 1,2,4-triazole unit shows signals at 10.035 and 6.5 ppm respectively.

The complex B containing phen units exhibit the chemical shift ranges from 7.596 - 8.865 ppm. The pyridine ring attached to the 5th position of 1,2,4-triazole ring present in the pytrzSH ligand show signals at 9.134 ppm for H^2, 8.45 ppm for H^4, 7.57 ppm for H^5 and 9.139 ppm for H^6 protons. The –SH group present in the 3rd position and the proton attached to the nitrogen atom at 4th position of 1,2,4-triazole ring shows signals at 9.994 and 6.995 ppm respectively. The ^1H NMR spectral data confirms the formation of complexes A and B (**Fig. S3**).

The ^{13}C NMR spectrum of complex A exhibits the carbon signals for bpy ligands is in the range 123-149 ppm. The carbon signals of phen ligands for complex B occur in the region 121-150 ppm. The ^{13}C NMR signals of pytrzSH ligand containing pyridine and 1,2,4-triazole rings occur in the region 121-170 ppm. In pytrzSH ligand, the C^3 atom of the pyridine ring is attached to the C^5 atom of the triazole ring. The C^3 atom of pyridine ring exhibits the carbon signal at 132.9 ppm for both the complexes. Similarly, the C^5 atom of the triazole ring displays the carbon signal at 158.6 and 156.1 ppm for complexes A and B. The C^3 atom attached to the –SH group of triazole ring shows a chemical shift at 164.6 and 169.5 ppm for complexes A and B.

3.1.5. Mass spectral analysis

The MALDI-TOF mass spectra of the synthesised complexes depict that the molecular ion, M^+ and the fragmentation peaks corresponds to the ruthenium metal coordinated with bpy, phen and pytrzSH ligands along with $(PF_6)_2$ counter ions. The molecular ion peak with loss of one and two PF_6^- counter ions shows an *m/z* value corresponding to M^{+-} PF_6^- and M^{+-} $2PF_6^-$ respectively. The *m/z* values of molecular and fragmentation ions obtained from the mass spectral data of complexes A and B are in good agreement with the theoretical values calculated from the molecular formula of the corresponding complexes (Table 1). Thus, the MALDI-TOF mass spectral data validate the assigned structure of the complexes A and B (**Fig. S4**).

3.2. Magnetic susceptibility, molar conductance and lipophilicity of complexes A and B

The synthesised complexes A and B coordinated with strong field ligands such as bpy, phen, and pytrzSH form low spin Ru^{2+} complexes of +2 oxidation state. The μ_{eff} value for the both the complexes obtained from the magnetic susceptibility measurements are less than 0 BM, hence, it is evident that the complexes A and B are said to be diamagnetic in nature. The molar conductance value of the synthesised complexes exhibits 180 and 190 Ω^{-1} cm^2 mol^{-1} for complexes A and B which clearly indicate the substitution of two monodentate ligands by the

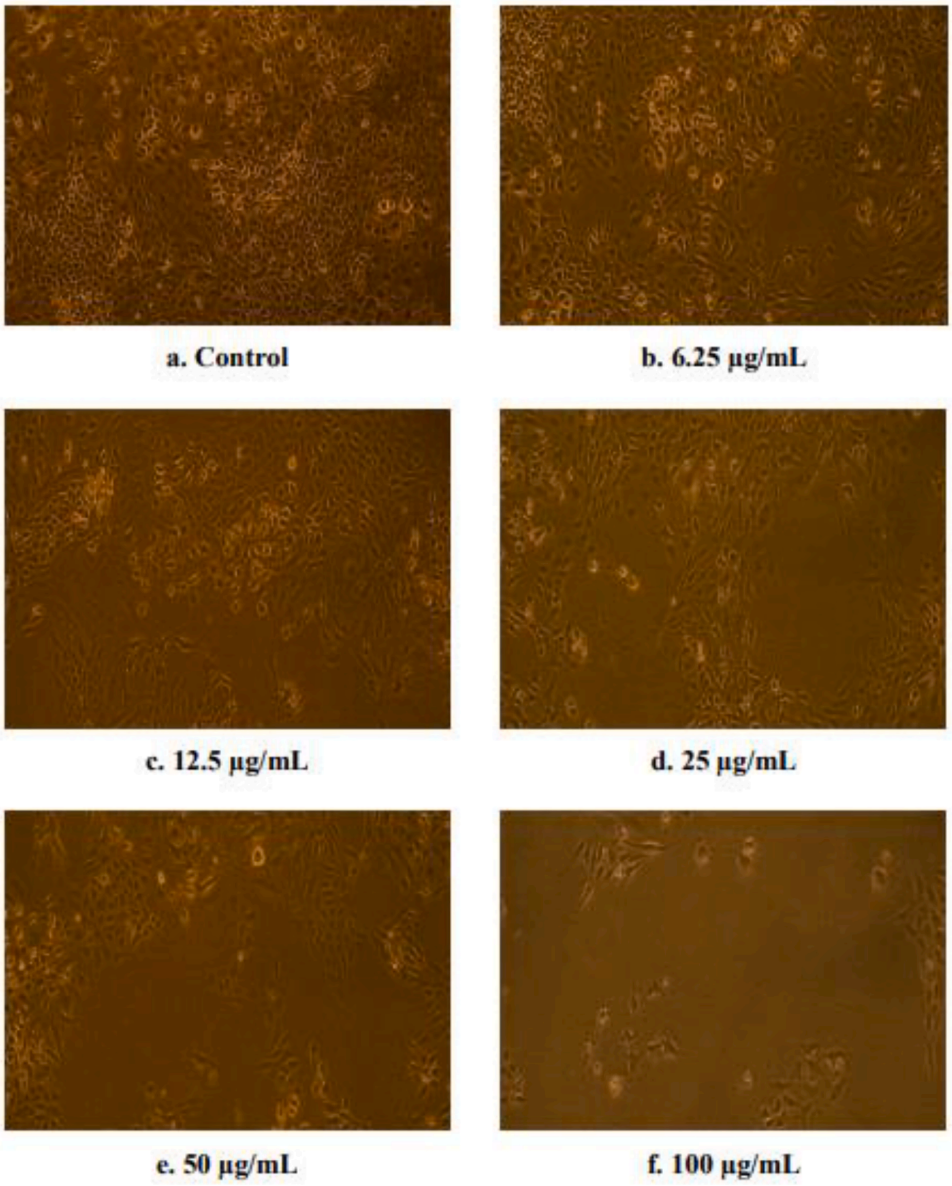

Fig. 6. Morphological changes of complex A on non-tumoral L6 cell line at various concentrations.

replacement of two chloride ions from the precursor complexes and it also point out the presence of two PF_6^- counter ions in the ratio 1:2. This also confirms the octahedral geometry of the synthesised complexes. The molar conductivity results reveal that both the synthesised complexes are non-electrolytic and suitable for biological studies. The pharmacokinetic properties and their interaction with the macromolecular target of the synthesised complexes are determined by the lipophilicity measurement. The lipophilicity of complexes A and B are quantified by the measurement of the partition coefficient, log *P* in octanol/water mixture and the values obtained is found to be 1.20 ± 0.00 for complex A and 1.86 ± 0.002 for complex B. The lipophilicity values also suggest that the synthesized complexes are appropriate for biological studies.

3.3. Biological evaluation of complexes A and B

3.3.1. Antimicrobial activity

Antibacterial activity of the PytrzSH ligand and the complexes A and B at 10 µg/mL are performed against *E. faecalis, S. aureus, P. aeruginosa* and *E. coli* and the zone of inhibition for the ligand and the complexes are tabulated in Table 2.

The pytrzSH ligand and the synthesised complexes shows no antibacterial activity against *E. faecalis*. On the other hand, the ligand and the complex A exhibit slight activity on *S. aureus, P. aeruginosa*. The ligand and the synthesised complexes display slight activity against the *E. coli*. The antibacterial activity of the intercalating ligands pytrzSH decreases on complexation with Ru(II) metal. Yang *et al.*, 2018 have reported that the gram-negative species show antimicrobial activity due to the inherent resistance to Ru(II) complexes containing polypyridine ligands [21]. Therefore, it is clear and evident that both the complexes A and B shows slight antibacterial activity on *E. coli* (Fig. 1). The antibacterial activity results indicate that the surfaces of the ligands and the complexes interact directly with the outer membrane of the human pathogens, causing the membrane to rupture and thus it kills the microbes.

Antifungal activity of the pytrzSH ligand and the synthesised complexes A and B are performed against two fungi *A. niger* and *C. albicans*. The results reveal that the synthesised complexes A and B show slight antifungal activity towards the selected fungi (Table 3). The complex A shows no antifungal activity towards *A. niger* whereas complex B

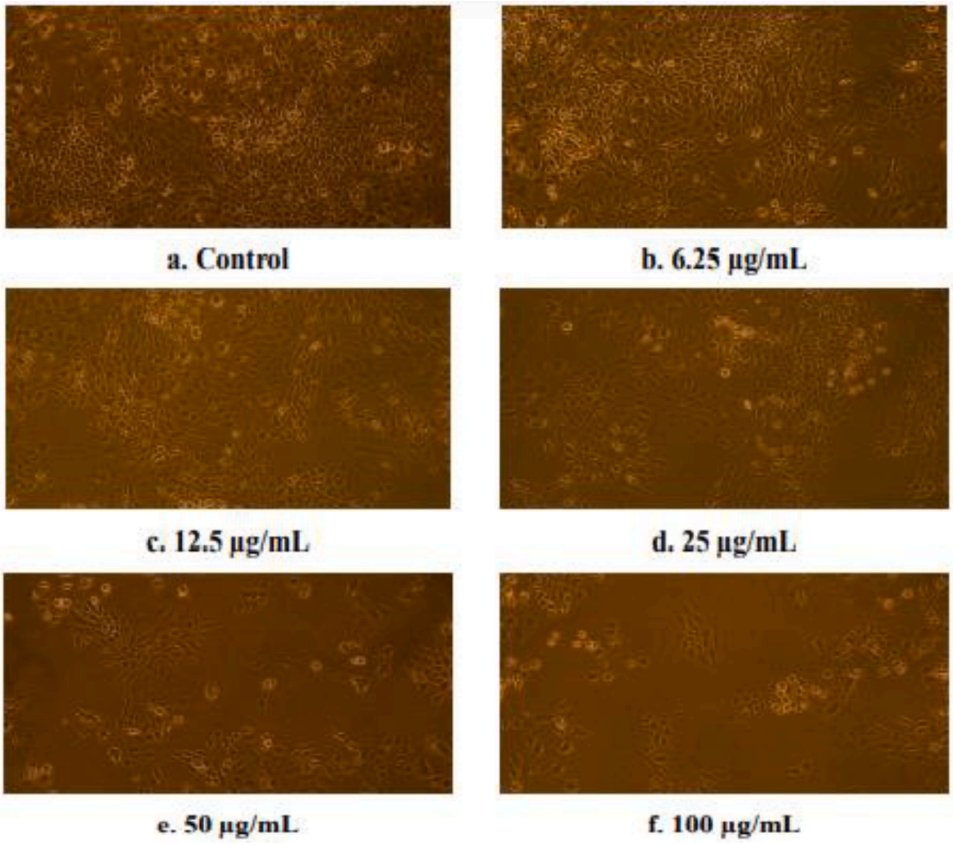

Fig. 7. Morphological changes of complex B on non-tumoral L6 cell line at various concentrations.

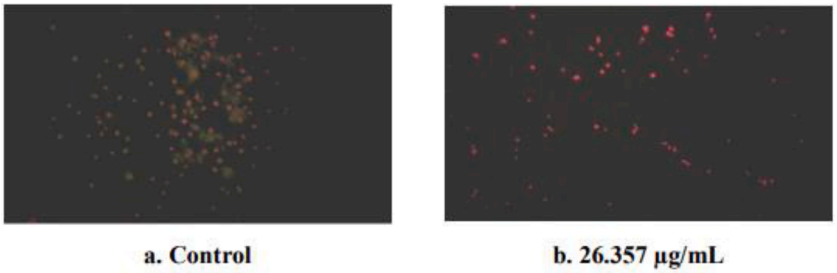

Fig. 8. Fluorescent microscopic images of control and complex A on SK-MEL-28 cell line.

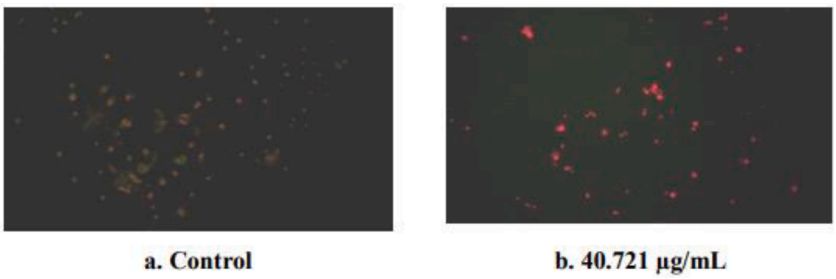

Fig. 9. Fluorescent microscopic images of control and complex B on SK-MEL-28 cell line.

complex shows slight antifungal activity towards both *A. niger* and *C. albicans*. On complexation of the pytrzSH ligand with $[Ru(bpy)_2Cl_2]$ and $[Ru(phen)_2Cl_2]$ precursors the antifungal activity may be the same or slightly increase, this change in activity depends on the nature of the coordinated ligands (Fig. 2).

The chelating ligands act as antimicrobial agent and thus inhibit the growth of microorganism. Upon complexation of this chelating ligands with the Ru(II) precursors, the lipophilic character increases and favours the penetration through the layer of microorganism membrane. The obtained results suggest that the synthesised complexes A and B possess

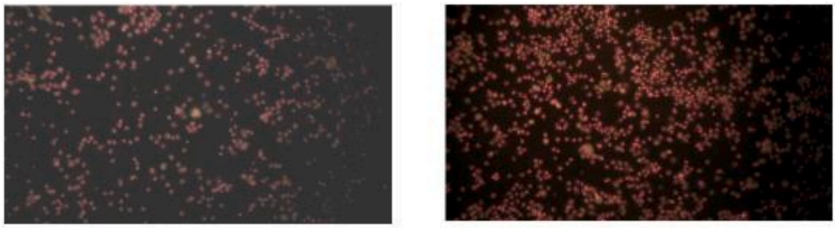

Fig. 10. Fluorescent microscopic images of control and complex A on non-tumoral L6 cell line.

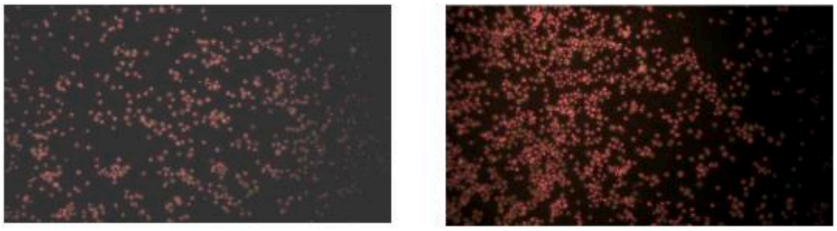

Fig. 11. Fluorescent microscopic images of control and complex B on non-tumoral L6 cell line.

Table 6
MTT assay of complex A on SK-MEL-28 cell line.

Complex A (µg/mL)	Response 1	Response 2	Response 3	Average	% cellular Viability	% growth Inhibition
0 (Control)	0.912	0.890	0.840	0.880	100	0
6.25	0.711	0.721	0.744	0.725	82.95	17.05
12.5	0.611	0.613	0.712	0.645	73.86	26.14
25	0.526	0.502	0.482	0.503	56.81	43.19
50	0.351	0.306	0.349	0.335	38.63	61.37
100	0.198	0.280	0.241	0.239	27.27	72.73

Table 7
MTT assay of complex B on SK-MEL-28 cell line.

Complex B (µg/mL)	Response 1	Response 2	Response 3	Average	% cellular Viability	% growth Inhibition
0 (Control)	0.812	0.837	0.851	0.833	100	0
6.25	0.736	0.771	0.740	0.749	90.36	9.64
12.5	0.713	.0715	0.682	0.703	84.33	15.67
25	0.517	0.565	0.543	0.541	65.06	34.94
50	0.328	0.355	0.372	0.351	42.16	57.84
100	0.200	0.161	0.160	0.173	20.48	79.52

Table 8
MTT assay of complex A on non-tumoral L6 cell line.

Complex A (µg/mL)	Response 1	Response 2	Response 3	Average	% cellular viability	% growth Inhibition
0 (Control)	0.718	0.731	0.712	0.72033	100	0
6.25	0.728	0.659	0.681	0.68933	95.83	4.17
12.5	0.629	0.635	0.551	0.605	84.72	15.28
25	0.421	0.491	0.419	0.44366	61.11	38.99
50	0.26	0.24	0.236	0.24533	34.72	65.28
100	0.129	0.159	0.208	0.16533	23.61	76.39

slight antimicrobial activity against the selected microorganisms. The changes in the antimicrobial strength of the complexes towards microorganism depend either on the impermeability of the cells of the microorganism or the difference in ribosome of microbial cells [34].

The synthesised complexes A and B show slight activity against bacteria and fungi taken in the present investigation this is due to the chelating property of the synthesised complexes. Chelation diminishes the polarity of the Ru(II) metal ions and thus it enhances the lipophilic

Table 9
MTT assay of complex B on non-tumoral L6 cell line.

Complex B (μg/mL)	Response 1	Response 2	Response 3	Average	% cellular viability	% growth Inhibition
0 (Control)	0.931	0.969	0.955	0.951	100	0
6.25	0.891	0.871	0.93	0.897	94.73	5.27
12.5	0.851	0.915	0.691	0.831	87.36	12.64
25	0.664	0.658	0.688	0.670	70.52	29.48
50	0.318	0.398	0.461	0.392	41.05	58.95
100	0.154	0.201	0.222	0.192	20	80

Table 10
IC_{50} values of complexes A and B on SK-MEL-28 and non-tumoral L6 cell lines.

Complex	IC_{50} on SK-MEL-28 cell line (μg/mL)	IC_{50} on non-tumoral L6 cell line (μg/mL)
Doxorubicin	4.97	7.943
Complex A	27.444	25.869
Complex B	40.721	38.425

nature of the complexes. Hence, the synthesised complexes diffuse through the cell membrane of the microorganisms and inhibit the growth of the organisms. This result is in accordance with the Tweedy's chelation theory [35].

3.3.2. Antidiabetic activity

The α-glucosidase inhibitory activity of the synthesised complexes A and B is determined at four different concentrations (25, 50, 100 and 200 μg/mL) at pH 6.9 against the positive control acarbose by measuring the absorbance of *p*-nitrophenol at 400 nm (Fig. 3). The IC_{50} value of the positive control acarbose is 231.55 μg/mL and this value is compared with the IC_{50} value of the synthesized complexes (Table 4).

The complex A shows higher IC_{50} value compared to the positive control acarbose and is not considered as an antidiabetic drug since its percentage of inhibition decreases from higher level to lower level as the complex concentrations increases. The π-π stacking interactions between the phen ligand and the electron rich substituted 1,2,4-triazole rings present in the complex B plays a vital role in the α-glucosidase inhibition leading to lower IC_{50} value. The absorbance value of complex B decreases as the concentration increases from 25 to 200 μg/mL, thus showing strong inhibition on α-glucosidase and is therefore considered as an antidiabetic drug.

The synthesised complexes show an appreciable α-glucosidase inhibitory effect in a concentration-dependent manner. The inhibition depends on the concentration of the substrate, enzyme and the duration of the incubation with the enzyme [36]. The absorbance and the percentage inhibition of α-glucosidase inhibitory assay for the complexes are tabulated in Table 5. The absorbance value for blank and control at 400 nm is 0.710 and 0.015.

Hence it is evident that the lower steric hindrance between the bpy substituted complex A and the pytrzSH ligand shows no α-glucosidase inhibitory activity, whereas π- π stacking interaction of phen substituted complex B shows moderate antidiabetic activity.

3.3.3. In vitro antiproliferative and cytotoxic effect of complexes A and B

The *in vitro* antiproliferative and cytotoxic evaluation of the synthesised complexes A and B are carried out by two-fold dilution of various concentrations (6.5, 12.5, 25, 50, 100 μg/mL) against the cancerous SK-MEL-28 and living non-cancerous L6 cell lines. The cellular morphological changes with respect to time and concentrations are monitored and recorded for both the cell lines. The absorbance values of the complexes on SK-MEL-28 melanoma and non-tumoral L6 cell lines are measured at 570 nm.

The percentage cellular viability of the complexes A and B are determined from the absorbance values by MTT assay method. The plot of percentage cellular viability *versus* concentration gives a sigmoidal response from which the IC_{50} value of the complexes are calculated. The average triplicate response carried out in MTT assay for both *in vitro* antiproliferative and cytotoxic effect of the complexes on SK-MEL-28 and non-tumoral L6 cell lines against the standard doxorubicin is calculated. The IC_{50} value of doxorubicin on SK-MEL-28 and non-tumoral L6 cell lines are determined by MTT assay and are calculated as 4.97 μg/mL and 7.943 μg/mL.

3.3.3.1. In vitro antiproliferative and cytotoxic activity of complexes A and B by direct microscopic method. *In vitro* antiproliferative and cytotoxic effects of complexes A and B at various concentrations on cancerous SK-MEL-28 and non-tumoral L6 cell lines along with DMEM are evaluated by direct microscopic method. The direct microscopic determination of complex A on SK-MEL-28 cancerous cells shows numerous morphological changes at various concentrations (Fig. 4). The treatment of 6.25 μg/mL of complex A on the cultured cancerous SK-MEL-28 cell lines exhibits an irregular elongation of the spindle shaped cells and shows reduction in the cell density. The increase in concentration of complex A from 6.25 to 12.5 μg/mL shows cell shrinkage and move towards the center with cell rupturing and loss of cellular fluid, where the cellular components floats on the surface of the cultured well plate. As the concentration of complex A increases from 25 to 100 μg/mL, there arise a maximum reduction in the number of cells from the periphery towards the center of the cultured well plate results in depletion of numerous cells which leads to cellular depletion and formation of vacuoles. The morphological changes that take place by the complex A on SK-MEL-28 cell line is due to the formation of reactive oxygen species (ROS). The changes in the cancerous SK-MEL-28 cell line due to the production of high intracellular ROS which normally disrupts the mitochondrial membrane potential. The loss of cell components and functions are accompanied by the ROS production leads to oxidative stress and ultimately lead to apoptosis [37]. This increase in ROS is due to the presence of 1,2,4-triazole moiety present in the synthesised complex A. The oxidative stress involves the abnormal cell growth in cancerous cells and a disruption of redox homeostasis due to either in the elevation in ROS production or a decline of ROS-scavenging capacity [38].

The complex B (6.25 and 12.5 μg/mL) on SK-MEL-28 cells shows initially a cell shrinkage, cluster formation of cells followed by the movement of cell clusters towards the periphery of the cell cultured plate (Fig. 5). As the concentration increases from 12.5 to 25 μg/mL there is a reduction in the size of the spindle shaped SK-MEL-28 cells which leads to irregular shaped cells with loss of cellular fluid. On further increase of complex B concentration from 50 to 100 μg/mL on SK-MEL-28 cells enormous number of cells get reduced and formation of cell vacuole leads to cell depletion. The changes in the structural and the morphology of the cancerous cells affect their anticancer activity of the synthesised complex B by tightly controlling the nature of their activation sites and their affinity towards the cellular target biomolecules thus leads to the lower antiproliferative activity.

3.3.3.2. Cytotoxic effect of complexes A and B on non-tumoral L6 cell line. The cytotoxic nature of complex A is determined by the incremental addition of various concentrations of complex A on non-tumoral

L6 cells (Fig. 6). The morphology of non-tumoral L6 line varies with respect to the concentration of complex A, at 6.25 and 12.5 μg/mL there is a decrease in minimum number of cells and the cellular fluid of the cells gets decreased in the center and move towards the periphery. Upon incremental addition of complex A from 25 to 50 μg/mL, cells get elongated and form irregular shape with loss of cell cytoplasm leading to vacuole formation and cell clusters. As the concentration of complex A further increase from 50 to 100 μg/mL there is an enormous depletion of cells with minimum cellular vacuoles present in the periphery of the cultured plate.

The complex B on non-tumoral L6 cells shows enormous changes in the cellular morphology and is mainly based on dose-dependent concentration (Fig. 7). The treatment of complex B with 6.25 μg/mL shows no marked changes. The reduction in the cellular fluid takes place at 12.5 μg/mL and therefore leads to change in the cellular size. The concentration at 25 μg/mL exhibit blebbing in the cells with minimum reduction of cells. As the concentration of complex B increases from 25 to 100 μg/mL on the non-tumoral L6 cell line numerous cellular lesions occurs and maximum number of cells gets reduced.

The same two-fold dilution concentration of the synthesised complexes A and B taken for direct microscopic method are further analyzed for MTT assay method on SK-MEL-28 and non-tumoral L6 cell lines in order to determine the IC_{50} value of the novel complexes A and B.

3.3.3.3. Antiproliferative and cytotoxic evaluation of complexes A and B using MTT assay method. Antiproliferative effect and cytotoxicity of complexes A and B are evaluated on SK-MEL-28 and non-tumoral L6 cell lines by MTT assay method and the results are tabulated in **Tables 6 - 9**. The percentage cellular viability decreases and the percentage growth inhibition increases with increases in concentration of the complexes in both the cell lines. The IC_{50} values obtained for complexes A and B on SK-MEL-28 cancerous cell line are found to be 27.444 and 40.721 μg/mL and for non-tumoral L6 cells are 25.869 and 38.425 μg/mL respectively (Table 10).

The results reveal that the complexes A and B show anticancer activity due to the presence of Ru(II)-bpy/phen moiety, which can lower the steric hindrance during their interaction with their biological targets and this may contribute to higher anticancer activities. This obtained result is in accordance with the anticancer activity of Ru(II)-polypyridyl complexes having (2-(4-(diethoxymethyl)−1H-imidazo[4,5-*f*]-[1,10]-phenanthroline) intercalating ligand performed on HeLa cell line and the IC_{50} values for the complexes are 39 ± 4.6 mM, 44.3 ± 6.3 mM and 49 ± 8 mM respectively [39]. The bpy and phen ligands present in the complexes A and B play an important role in the anticancer activity on SK-MEL-28 cell line. Zhang et al., reported that Ru(II)-polypyridine complexes having ancillary bpy/phen ligand plays a major role in the anticancer activity of various cell lines [40]. The anticancer activity of the complexes A and B is also due to the presence of the intercalating pytrzSH ligand. The thiol group present in the triazole moiety produces thiyl radicals which are readily formed by the homolytic cleavage of S-H bond at 87 $kcalmol^{-1}$ [41]. The thiyl radicals formed from the thiol groups of the complexes A and B act as a chain transfer agent and maintain an intracellular homeostasis because of its high reactivity and low bond dissociation energy of S-H bond [42]. The triazole ring is linked at the 3rd position of the pyridine moiety and –SH group is substituted in the 3rd position of triazole nucleus suggesting the complexes A and B displaying higher cytotoxic activities.

3.3.3.4. Apoptotic effect of complexes A and B on SK-MEL-28 and non-tumoral L6 cell line. The PCD at 27.444 μg/mL of complex A and 40.721 μg/mL of complex B on SK-MEL-28 cell line show late apoptotic effect (Figs. 8 and 9). This late apoptotic effect on complexes A and B are indicated by the bright orange-stained nuclei. This late apoptotic nature of the complexes is mainly based on the IC_{50} concentration. The pyridyl ring substituted in the 1,2,4-triazole ring makes the mitochondrial membrane potential disruption leads to the release of cytochrome C into the cytoplasm leading to late apoptotic effect [43].

The apoptotic nature of the complexes A and B are analyzed on non-tumoral L6 cell line at IC_{50} values and the results clearly depict that these complexes show early apoptotic effect by bright green-stained nuclei with chromatin condensation. The fluorescent microscopic images display early apoptotic nature in both the complexes (Figs. 10 and 11)

The synthesised complexes A and B containing pyridine substitution in the 3rd position of 1,2,4-triazole ring leads to the apoptotic cell death. Therefore, it is evident and clear that N,N chelating ligands in complexes A and B shows mitochondrial dysfunction and trigger intrinsic apoptotic pathways in non-tumoral L6 cell line through extended cytoplasm and nuclear condensation [44]. The IC_{50} concentrations of complexes A and B stained with AO/EB shows dead and floating cells exhibiting early apoptotic effect on viable cells (Table 6,Table 7,Table 8,Table 9).

4. Conclusion

The biological activity *viz* antimicrobial, antidiabetic and anticancer activities of the synthesised complexes against the control are carried out by agar disk diffusion, α- glucosidase inhibitory assay and MTT methods. The pytrzSH ligand and the synthesised complexes exhibit slight antimicrobial activity of selected bacteria and fungi. The antidiabetic activity of the complexes A and B is determined from the IC_{50} values and its if found to be 490.32 and 223.01 μg/mL. The changes in the morphology of SK-MEL-28 and non-tumoral L6 cell lines in the presence of the complexes A and B are determined by direct microscopic method and are purely based on concentration through dose and time-dependent manner. The complexes A and B show lower antiproliferative and higher cytotoxic effect on the selected cell lines. The PCD using AO/EB double staining method based on the IC_{50} values for both the complexes A and B shows late apoptotic effect on SK-MEL-28 cell line and early apoptotic effect on the non-tumoral L6 cell line. The obtained results indicate that the antiproliferative and cytotoxic activities of the synthesised complexes depend on the concentration of the complexes and the nature of the ligands present in the complexes.

Financial support and sponsorship

The authors did not receive support from any organization for the submitted work.

Ethical statement

This material is the authors' own original work, which has not been previously published elsewhere.

Human/animal rights

This article does not contain any studies with human or animal subjects performed by the any of the authors.

CRediT authorship contribution statement

Santhiya S: Formal analysis, Writing – original draft, Writing – review & editing, Methodology, Validation, Investigation. **Arul Mary S:** Writing – review & editing. **Sheeba Daniel:** Writing – review & editing, Conceptualization, Investigation, Resources, Supervision.

Declaration of Competing Interest

The authors declare that they have no known competing financial interests or personal relationships that could have appeared to influence the work reported in this paper.

Data availability

Data will be made available on request.

Supplementary materials

Supplementary material associated with this article can be found, in the online version, at doi:10.1016/j.chphi.2023.100424.

References

[1] H.K.P. Porto, C.A.S.T. Vilanova-Costa, F.M.S. Mello, W.L. Costa, A.P. Lima, F. C. Pereira, M.A.P. Almeida, A.E. Graminha, A.A. Batista, E.P. Silveira-Lacerda, Synthesis of a ruthenium(II) tryptophan-associated complex and biological evaluation against Ehrlich murine breast carcinoma, Transition Met. Chem. 40 (2015) 1–10, https://doi.org/10.1007/s11243-014-9882-1.

[2] M. Frezza, S. Hindo, D. Chen, A. Davenport, S. Schmitt, D. Tomco, P. Dou, Novel metals and metal complexes as platforms for cancer therapy, Curr. Pharm. Des. 16 (2010) 1813–1825, https://doi.org/10.2174/138161210791209009.

[3] D. Gopalakrishnan, M. Ganeshpandian, R. Loganathan, N.S.P. Bhuvanesh, X. J. Sabina, J. Karthikeyan, Water soluble Ru(II)–arene complexes of the antidiabetic drug metformin: DNA and protein binding, molecular docking, cytotoxicity and apoptosis-inducing activity, RSC Adv. 7 (2017) 37706–37719, https://doi.org/10.1039/C7RA06514K.

[4] S. Rafique, M. Idrees, A. Nasim, H. Akbar, A. Athar, Transition metal complexes as potential therapeutic agents, Biotechnol. Mol. Biol. Rev. 5 (2010) 38–45, https://doi.org/10.1039/C9TB02669J.

[5] E. Boros, P.J. Dyson, Classification of metal-based drugs according to their mechanisms of action, Chem 6 (2020) 41–60, https://doi.org/10.1016/j.chempr.2019.10.013.

[6] P.C.A. Bruijnincx, P.J. Sadler, New trends for metal complexes with anticancer activity, Curr. Opin. Chem. Biol. 12 (2008) 197–206, https://doi.org/10.1016/j.cbpa.2007.11.013.

[7] R. Kaushal, Sheetal, In vitro anticancer and antibacterial activities of octahedral ruthenium(III) complexes with hydroxamic acids. Synthesis and spectroscopic characterization, Russ. J. Gen. Chem. 86 (2016) 360–367, https://doi.org/10.1134/S1070363216020274.

[8] G. Gasser, N.M. Nolte, The potential of organometallic complexes in medicinal chemistry, Curr. Opin. Chem. Biol. 16 (2012) 84–91, https://doi.org/10.1016/j.cbpa.2012.01.013.

[9] M.V.S. Amaral, A.J.D.S. Portilho, E.L.D. Silva, L.D.O. Sales, H.D.S.Maués J, MA.E. D. Moraes, C.A. Moreira-Nunes, Establishment of drug-resistant cell lines as a model in experimental oncology: A review, Anticancer Res. 39 (2010) 6443–6455, https://doi.org/10.21873/anticanres.13858.

[10] A.M. Florea, D. Büsselberg, Cisplatin as an anti-tumor drug: Cellular mechanisms of activity, drug resistance and induced side effect, Cancers (Basel) 1 (2011) 1351–1371, https://doi.org/10.3390/cancers3011351.

[11] U. Ndagi, M.E.Soliman N.Mhlongo, Metal complexes in cancer theraphy-an update from drug design perspective, Drug Des. Devel. Ther. 11 (2017) 599–616, https://doi.org/10.2147/DDDT.S119488.

[12] I. Kostova, Ruthenium complexes as anticancer agents, Curr. Med. Chem. 13 (2006) 1085–1107, https://doi.org/10.2147/DDDT.S275007.

[13] E.S. Antonarakis, A. Emadi, Ruthenium-based chemotherapeutics: are they ready for prime time, Cancer Chemother. Pharmacol. 66 (2010) 1–9, https://doi.org/10.1007/s00280-010-1293-1.

[14] A.J. Mason, A. Marquette, B. Bechinger, Zwitterionic phospholipids and sterols modulate antimicrobial peptide-induced membrane destabilization, Biophys. J. 93 (2007) 4289–4299, https://doi.org/10.1529/biophysj.107.116681.

[15] H. Sakurai, A. Katoh, T. Kiss, T. Jakusch, M. Hattori, Metallo-allixinate complexes with anti-diabetic and anti-metabolic syndrome activities, Metallomics 2 (2010) 670–682, https://doi.org/10.1039/c0mt00025f.

[16] S. Maikoo, D. Makayane, I.N. Booysen, P. Ngubane, A. Khathi, Ruthenium compounds as potential therapeutic agents for Type 2 Diabetes Mellitus, Eur. J. Med. Chem. 1 (2020) 1–30, https://doi.org/10.1016/j.ejmech.2020.113064.

[17] W.H. Ang, G.Sava A.Casini, P.J. Dyson, Organometallic ruthenium-based antitumor compounds with novel modes of action, J. Organomet. Chem. 696 (2011) 989–998, https://doi.org/10.1016/j.jorganchem.2010.11.009.

[18] P. Zhang, P.J. Sadler, Redox-active metal complexes for anticancer therapy, Eur. J. Inorg. Chem. 12 (2017) 1541–1548, https://doi.org/10.1002/ejic.201600908.

[19] G.K. Gransbury, P. Kappen, C.J. Glover, J.N. Hughes, A. Levina, P.A. Lay, L. F. Musgravee, H.H. Harris, Comparison of KP1019 and NAMI-A in tumour-mimetic environments, Metallomics 8 (2016) 762–773, https://doi.org/10.1039/c6mt00145a.

[20] F.P. Dwyer, E.C. Gyarfas, W.P. Rogers, J.H. Koch, Biological activity of complex ions, Nature 170 (1952) 190–191, https://doi.org/10.1038/170190a0.

[21] Y. Yang, G. Liao, C. Fu, Recent advances on octahedral polypyridyl ruthenium(II) complexes as antimicrobial agents, Polymers 10 (2018) 1–12, https://doi.org/10.3390/polym10060650.

[22] T. Pivarcsik, O. Dömötör, J.P. Mészáros, N.V. May, G. Spengler, O. Csuvik, I. Szatmári, E.A. Enyedy, 8-Hydroxyquinoline-amino acid hybrids and their half-sandwich Rh and Ru complexes: Synthesis, anticancer activities, solution chemistry and interaction with biomolecules, Int. J. Mol. Sci. (2021) 1–29, https://doi.org/10.3390/ijms222011281, 22.

[23] C. Molinaro, A. Martoriati, K. Cailliau, Proteins from the DNA damage response: Regulation, dysfunction, and anticancer strategies, Cancers 12 (2021) 1–39, https://doi.org/10.3390/cancers13153819.

[24] S.C. Holm, B.F. Straub, Synthesis of n-substituted 1,2,4-triazoles. A review, Org. Prep. Proced. Int. 43 (2011) 319–347, https://doi.org/10.1080/00304948.2011.593999.

[25] M.J. Marmura, S.D. Silberstein, T.J. Schwedt, The acute treatment of migraine in adults: The American Headache Society Evidence Assessment of Migraine Pharmacotherapies, Headache J. Head Face Pain 55 (2015) 3–20, https://doi.org/10.1111/head.12499.

[26] M.H. Klingele, P.D.W. Boyd, B. Moubaraki, K.S. Murray, S. Brooker, Probing the dinucleating behaviour of a bis-bidentate ligand: Synthesis and characterisation of some di- and mononuclear Cobalt(II), Nickel(II), Copper(II) and Zinc(II) complexes of 3,5-di(2-pyridyl)-4-(1H-pyrrol-1-yl)- 4H1,2,4-triazole, Eur. J. Inorg. Chem. 2006 (2006) 573–589.

[27] A. Muleya, K.S. Karumban, P. Gupta, S. Kumbhakar, B. Giri, R. Raut, A. Misra, S. Maji, Synthesis, structure, spectral, redox properties and anti-cancer activity of Ruthenium(II) Arene complexes with substituted Triazole Ligands, J. Organomet. Chem. 954 (2021) 1–14.

[28] A.A.M. El-Reedy, N.K. Soliman, Synthesis, biological activity and molecular modelling study of novel 1,2,4-triazolo[4,3-b]-[1,2,4,5]-tetrazines and 1,2,4-triazolo[4,3-b]-[1,2,4]-triazines, Sci. Rep. 10 (2020) 1–18.

[29] M.K. Trivedi, R.M. Tallapragada, A. Branton, D. Trivedi, G. Nayak, R. Mishra, S. Jana, Characterization of physical, spectral and thermal properties of biofield treated 1,2,4-triazole, J. Mol. Pharm. Org. Process. Res. 3 (2015) 100–128.

[30] N. Gligorijević, S. Aranđelović, L. Filipović, K. Jakovljević, R. JankovićS. Grgurić-Šipka, I. Ivanović, S. Radulović, Z.L. Tešić, Picolinate ruthenium(II)-arene complex with in vitro antiproliferative and antimetastatic properties: Comparison to a series of ruthenium(II)-arene complexes with similar structure, J. Inorg. Biochem. 108 (2012) 53–61, https://doi.org/10.1016/j.jinorgbio.2011.12.002.

[31] A. Hussain, M.F. AlAjmi, M.T. Rehman, A.A. Khan, P.A. Shaikh, R.A. Khan, Evaluation of transition metal complexes of benzimidazole-derived scaffold as promising anticancer chemotherapeutics, Molecules 23 (2018) 1–18, https://doi.org/10.3390/molecules23051232.

[32] S.Y. Sun, R.J. r Mh, Lotan, Apoptosis as a novel target for cancer chemoprevention, J. Natl. Cancer Inst. 96 (2004) 662–672, https://doi.org/10.1093/jnci/djh123.

[33] H.L. Yang, C.S. Chen, W.H. Chang, F.J. Lu, Y.C. Lai, C.C. Chen, T.H. Hseu, C.T. Kuo, Y.C. Hseu, Growth inhibition and induction of apoptosis in MCF-7 breast cancer cells by Antrodia camphorate, Cancer Lett. 231 (2006) 215–227, https://doi.org/10.1016/j.canlet.2005.02.004.

[34] Y.P. Kumar, C.S. Devi, A. Srishailam, N. Deepika, V.R. Kumar, P.V. Reddy, K. Nagasuryaprasad, S.S. Singh, P. Nagababu, S. Satyanarayana, Studies on photocleavage, DNA binding, cytotoxicity, and docking studies of ruthenium(II) mixed ligand complexes, J. Fluoresc. 26 (2006) 2119–2132, https://doi.org/10.1007/s1085-016-108y.

[35] S.K. Balakrishnan, S.K. Dass, H.A.D. Rajendran, I. Savrimuthu, Cytotoxicity and antimicrobial activity of mono-, di- and trinuclear ruthenium(II) polypyridine complexes, Int. J. Pharma. Sci. 7 (2014) 317–321.

[36] Y.G. Chen, P. Li, R. Yan, X.Q. Zhang, Y. Wang, X.T. Zhang, W.C. Ye, Q.W. Zhang, α-Glucosidase inhibitory effect and simultaneous quantification of three major flavonoid glycosides in Microctis folium, Molecules 18 (2013) 4221–4232, https://doi.org/10.3390/molecules18044221, 2013.

[37] R. Zhang, I. Humphreys, R.P. Sahu, Y. Shi, S.K. Srivastava, In vitro and in vivo induction of apoptosis by capsaicin in pancreatic cancer cells is mediated through ROS generation and mitochondrial death pathway, Apoptosis 13 (2008) 1465–1478, https://doi.org/10.1007/s10495-008-0278-6.

[38] D. Trachootham, J. Alexandre, P. Huang, Targeting cancer cells by ROS-mediated mechanisms: A radical therapeutic approach? Nat. Rev. Drug Discov. 8 (2009) 579–591, https://doi.org/10.1038/nrd2803.

[39] R.K. Vuradi, K. Dandu, P.K. Yata, R.R. Mallepally, N. Chintakuntla, R. Ch, S. S. Thakur, C.M. Rao, S. Satyanarayana, Studies on the DNA binding and anticancer activity of Ru(II) polypyridyl complexes by using a (2-(4-(diethoxymethyl)-1H-imidazo[4,5-f][1,10]phenanthroline)) intercalative ligand, New J. Chem. 42 (2018) 846–859, https://doi.org/10.1039/C9NJ90103E.

[40] C. Zhang, B.J. Han, C.C. Zeng, S.H. Lai, W. Li, B. Tang, D. Wan, G.B. Jiang, Y.J. Liu, Synthesis, characterization, in vitro cytotoxicity and anticancer effects of ruthenium(II) complexes on BEL-7402 cells, J. Inorg. Biochem. 157 (2016) 62–72.

[41] M.D. Nolan, E.M. Scanlan, Applications of thiol-ene chemistry for peptide science, Front. Chem. 8 (2020) 1–21.

[42] M.H. Ahmad, N.A. Rahman, F.A. Kadir, L.A. Al-Ani, N.M. Hashim, W.A. Yehye, Design and synthesis of sulfur-containing butylated hydroxytoluene: Antioxidant potency and selective anticancer agent, J. Chem. Sci. 131 (2019) 1–11.

[43] J.J. Wang, W. Zhang, B.J.S. Sanderson, Altered mRNA expression related to the apoptotic effect of three xanthones on human melanoma SK-MEL-28 cell line, Biomed. Res. Int. 1 (2013) 1–10, https://doi.org/10.1155/2013/715603.

[44] T. Chen, Y. Liu, W.J. Zheng, J. Liu, Y.S. Wong, Ruthenium polypyridyl complexes that induce mitochondria-mediated apoptosis in cancer cells, Inorg. Chem. 49 (2010) (2010) 6366–6368, https://doi.org/10.1021/ic100277w.